International Journal for Housing Science and Its Applications
Publish August 6, 2025. Volume 46, Issue 3 Pages 4864-4873

https://doi.org/10.70517/ijhsa463416

Research on current measurement error compensation technology of standard energy meter based on large-scale data mining

Xingzhi Liu[1,2,*], Wenbo Yao[1], Juan Tian[1] and Yu Su[1]
[1] State Grid Chongqing Electric Power Company Marketing Service Center, Chongqing, 401123, China
[2] School of Electrical Engineering, Chongqing University, Chongqing, 400030, China
Corresponding authors: (e-mail: 18084020531@163.com).

Abstract In space vehicles, inertial navigation devices need to measure real-time and high-precision analog quantities such as currents and voltages output from accelerometers and other sensors in order to realize the navigation of the vehicle. Therefore, it is of great significance to develop a dynamic high-precision current and voltage measurement system suitable for use in spacecraft. The study firstly designs a current error monitoring system, and then introduces the main factors affecting the measurement accuracy of a standard power meter and explores the principle of current measurement error generation. Then, a compensation strategy for segmental integration of the d-axis current into the measured current is proposed. The simulation and experimental results show that the current monitoring system can effectively eliminate the interference of the outer-loop controller and significantly improve the control performance of the error compensator, and the compensation algorithm proposed in this paper can effectively reduce the measurement error of the measured sub-current and improve the steady state and dynamic performance of the machine speed control system.

Index Terms current measurement, measurement error, error compensation, monitoring control system

I. Introduction

Current measurement, is the basis of power production and fair trading of electricity [1]. Measurement of the main parameters involved in electric power, such as current, voltage, active/reactive power, frequency, phase, electrical energy, harmonics, etc., is the data source and basis for protection control, automatic control, system operation scheduling, equipment control, energy saving and consumption reduction, and fine management in the power system, and the measurement level of these parameters will directly affect the operation quality of the power system [2]-[5]. Correspondingly, the accurate measurement of electric energy is an important link in the production and management of electric power enterprises and the stable operation of the power grid economy, and it is the basic guarantee for the grid company to carry out the fair trade of electric energy, so the standard power meter plays a vital role in the field of electric power production [6]-[8].

Measurement accuracy is an important indicator to characterize the long-term stable operation of the standard energy meter, however, there is, in the actual use of the process may appear instrument drift, stability does not meet the requirements and other issues [9], [10]. Currently commercial standard power meter accuracy is mostly in the 0.2 ~ 1.0 level, its measurement device that is the standard power meter accuracy of 0.05 level, to calibrate the accuracy of the standard power meter, the accuracy of the calibration device needs to be better than 0.01 level [11], [12]. Stability is the assessment of the standard power meter is extremely important technical indicators, analyze the standard power meter value over time of long-term slow changes, explore the impact of the accuracy index change factors, the impact of the amount of influence of the relationship between the degree of influence, to ensure that high-precision standard meter of long-term accuracy, stable operation, is of great importance [13]-[15].

The study firstly proposes a monitoring control system based on current measurement, and then introduces the main influencing factors affecting the accuracy of standard current measurement and the principle of current error generation. And in order to reduce the influence of gain error and measurement error on the current control system, a compensation strategy of segmental integration of the d-axis current is proposed, and the error term is obtained by integrating the d-axis current, which is compensated into the measurement current. The monitoring system in this paper includes abnormal data mining of current measurement, abnormal data error compensation control and measurement data implementation monitoring, and finally the effectiveness and practicality of the method in this paper is verified by simulation experiments.

II. Software design of the error control monitoring system

II. A.Anomaly data mining based on current measurements

When mining the abnormal data of current measurement, it mainly targets the current measurement results, flow rate measurement results and flow rate measurement results. Before the error control of current measurement data, it is necessary to define the criteria for judging the data error, and combined with the current characteristics, the following definition expression is derived:

$$W = e\left[-\log q\right] = -\sum_{i=1}^{n} q \log q \tag{1}$$

where, W is the data error standard defined and quantified by this paper; e is the statistical average of the uncertainty of the error data; q is the specific probability of anomalous data during the current measurement process; n is the number of information elements and probabilistic events that are contained in a current measurement device.

For the current measurement data contains all kinds of content and characteristic attributes, its specific value range needs to be decided according to the specific measurement imposed interval. Therefore, this paper combines the quantization method in current measurement technology to quantify the possible distribution characteristics of the anomaly data. The looseness of the distribution of the characteristics of the anomalous data is quantified, so as to obtain the corresponding change response of the measurement equipment when the anomalous data is output.

Define all the attribute characteristics of the anomalous data, denoted by M. P_{ij} is then expressed as the size of the j value of the i anomalous data feature attribute. In mining the anomalous data in the current measurement results, the following expression is derived:

$$r = \sum_{j=1}^{z_i} P_{ij} \tag{2}$$

where, r all the measurement result data of a certain attribute i; z_i is the number of all corresponding anomalies among a certain attribute i.

II. B.Abnormal data error compensation control

After completing the mining of anomalous data, the corresponding error compensation control, combined with the sensor measurement device to obtain the corresponding pressure parameters, the sensor output will not only be associated with the pressure, but also by the water conservancy project around the influence of the environmental temperature. Therefore, in order to avoid the influence of the ambient temperature on the error compensation, the system also needs to be combined with the temperature changes in the abnormal data for nonlinear compensation, and in the process of control according to the pressure changes in the compensation value for automatic adjustment. In order to achieve the above compensation control purpose, combined with neural network technology [16], set the system to measure the input of the sensor in the device and the surrounding ambient temperature as the input data of the neural network, and utilize the ability of the neural network to approximate any nonlinearities to achieve the error compensation of the anomalous data. Before the compensation, it is also necessary to connect the output data of multiple sensors with the corresponding ambient temperature data under different pressure and temperature conditions, introduce them into the neural network, and train the neural network by using the data measured by the standard manometer as the standard output mode to ensure that the input and output values of the neural network can conform to a certain mapping relationship. When the training of the neural network is completed, due to its generalization ability, even if the input data is untrained data, the system can also make the system output reasonable results.

II. C.Real-time monitoring of current measurement data

In order to ensure the continuity of the measurement error compensation control [17], it is also necessary to introduce a real-time monitoring module for current measurement data in the system of this paper. The introduction of port scanning, measurement device scanning, measurement data material and other operations and behaviors in this system can cause the error compensation to appear abnormal phenomena. In order to effectively avoid this phenomenon, the system in this paper carries out real-time monitoring and calculation of the transmission protocol corresponding to the measured data, so as to match the attributes of the abnormal data, and ensure the accuracy of judging the type of abnormal data.

III. Compensation for current measurement errors in standard energy meters

III. A. Main Factors Affecting the Measurement Accuracy of Standard Energy Meters

III. A. 1) Principle of the energy measurement unit of a standard energy meter

Standard power meter measurement unit is mainly divided into digital and analog measurement principle. As the digital measurement unit has the technical advantages of high precision, small start-up current, good electromagnetic compatibility, strong resistance to external magnetic field interference, and good functional scalability compared with the analog measurement unit, the digital measurement principle is commonly used in the standard power meter at present. Digital measurement unit is mainly composed of U/U voltage conversion circuit, I/U current conversion circuit, AD signal acquisition circuit, reference signal, standard clock and other parts. The main role of the power measurement unit is to transform the input voltage and current into a pulse signal proportional to the power, sent to the frequency division and counting. The power measurement unit is the key to the standard power meter, and its measurement accuracy directly determines the measurement accuracy of the power meter. The schematic block diagram is shown in Figure 1.

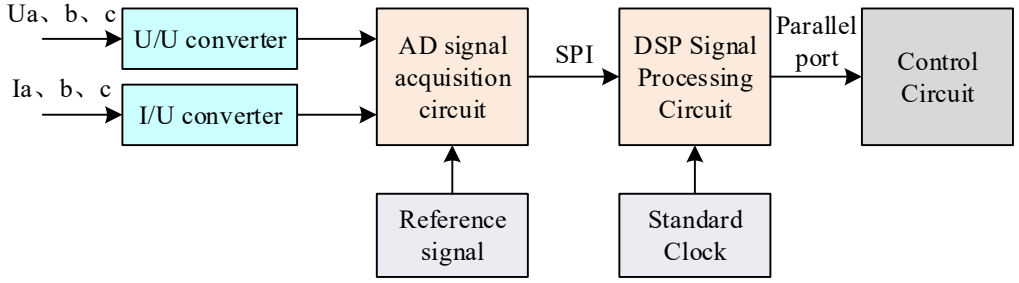

Figure 1: The principle of the standard electric energy meter is a block diagram

III. A. 2) U/U voltage conversion circuits

Voltage channel converter circuits currently have two main sampling circuit methods, respectively, the use of resistance voltage divider converter circuits and voltage transformer converter circuit form.

III. A. 3) I/U current conversion circuits

Current channel conversion circuit and voltage, there are currently two main sampling circuit, respectively, the use of resistance shunt conversion circuit or current transformer conversion circuit form.

III. A. 4) AD signal acquisition circuit

AD signal acquisition circuit core for the AD sampling chip, AD sampling chip is divided into a variety of commonly used types of parallel comparison type, successive approximation type, integral type, Σ-$\square$ modulation type, voltage-frequency conversion type and capacitance array successive comparisons; generally the higher the speed, the higher the accuracy. Different sampling methods of long-term stability impact parameters are not the same, but the main impact of the larger amount of indicators is the temperature drift. With the development of electronic technology, many AD chips now have integrated temperature sensors, in the DSP algorithm according to the temperature drift curve provided by the chip supplier to introduce a correction curve coefficient can effectively improve the reduction of AD by the temperature impact of long-term stability indicators.

III. B. Analysis of Current Measurement Gain Errors

III. B. 1) Current Gain Errors

The current gain error is mainly due to the gain error of the op-amp and the full scale error of the AD causing the gain of the A and B circuits to be inconsistent during the phase current measurement. The current measurement values are shown in the following equation:

$$\begin{aligned} I_{a\_measure} &= A_a I_a \\ I_{b\_measure} &= A_b I_b \\ I_{c\_measure} &= -\left(I_{a\_measure} + I_{b\_measure}\right) \end{aligned} \tag{3}$$

where, $I_{a,b,c\_measure}$ is the measured value of phase current; A_a, A_b are the gains of A, B phase currents, respectively; and $I_{a,b,c}$ is the actual current value.

The dq -axis current obtained by the Clark/Park transform is:

$$\begin{aligned} I_d &= I_a \cos\theta_{elec} + \frac{I_a + 2I_b}{\sqrt{3}} \sin\theta_{elec} \\ I_q &= -I_a \sin\theta_{elec} + \frac{I_a + 2I_b}{\sqrt{3}} \cos\theta_{elec} \end{aligned} \tag{4}$$

This leads to the following equation for the current fluctuation caused by the three-phase PMSM current gain error:

$$\begin{aligned} \Delta I_d &= \left(I_a - I_{a\_measure}\right)\cos\theta_{elec} + \frac{\left(I_a - I_{a\_measure}\right) + 2\left(I_b - I_{b\_measure}\right)}{\sqrt{3}} \sin\theta_{elec} \\ \Delta I_q &= \left(I_{a\_measure} - I_a\right)\sin\theta_{elec} + \frac{\left(I_a - I_{a\_measure}\right) + 2\left(I_b - I_{a\_measure}\right)}{\sqrt{3}} \cos\theta_{elec} \end{aligned} \tag{5}$$

III. B. 2) Current Bias Errors

The current bias error is mainly the bias voltage and zero error of the op amp and AD converter. The current measurements are shown in the following equation:

$$\begin{aligned} I_{a\_measure} &= I_a + I_{offset\_a} \\ I_{b\_measure} &= I_b + I_{offset\_b} \\ I_{c\_measure} &= -\left(I_{a\_measure} + I_{b\_measure}\right) \end{aligned} \tag{6}$$

where, I_{offset_a}, I_{offset_b} are the A, B phase current bias error respectively.

The current fluctuation caused by the three-phase PMSM current bias error can be derived from equation (6) as follows:

$$\begin{aligned} \Delta I_d &= I_{offset\_a} \cos\theta_{elec} + \frac{I_{offset\_a} + 2I_{offset\_b}}{\sqrt{3}} \sin\theta_{elec} \\ \Delta I_q &= I_{offset\_a} \sin\theta_{elec} + \frac{I_{offset\_a} + 2I_{offset\_b}}{\sqrt{3}} \cos\theta_{elec} \end{aligned} \tag{7}$$

III. C. Current measurement error compensation strategy

III. C. 1) Calculation of measurement errors

The output of the d axis current after passing through the integral regulator is:

$$i_{out} = k_{ci} \int_0^t \left(i_d^* - i_d^m\right) dt = -k_c \int_0^t \Delta i_d \, dt \tag{8}$$

The d axis measurement error Δi_{d} in Eq. (8) is the sum.

The pulsation of the d axis current contains the pulsation at the frequency of f_e, $2f_e$, so in this paper, we choose the integration interval of i_{out} to be $[0, 2\pi]$, and the integral of i_{out} is a constant value of the offset error and the gain error.

III. C. 2) Offset Error Calculation

Integrating Eq. (8) and choosing every π electrical angle for the integration interval, we have:

$$\sec 1 = \int_0^{\pi} \int_0^t -k_{ci} \Delta i_d \, dt d\theta_e = -2\frac{k_{ci}}{\omega_e} \Delta i_a \tag{9}$$

$$\sec 2 = \int_{\pi}^{2\pi} \int_0^t -k_{ci} \Delta i_d \, dt d\theta_e = 2\frac{k_{ci}}{\omega_e} \Delta i_a \tag{10}$$

Subtracting equations (9) and (10) gives:

$$\varepsilon_1 = \sec 1 - \sec 2 = -4\frac{k_{ci}}{\omega_e}\Delta i_a \tag{11}$$

Controlling Eq. (11) to zero eliminates the effect of the A phase offset error on the phase current measurement results.

Integrating Eq. (8) and choosing every $\pi/3$ electrical angle for the integration interval gives:

$$\begin{aligned}
\sec I &= \int_0^{\frac{\pi}{3}}\int_0^t -k_{ci}\Delta i_{d_offset}dtd\theta_e = \frac{k_{ci}}{\omega_e}\Delta i_b \\
\sec II &= \int_{\frac{\pi}{3}}^{\frac{2\pi}{3}}\int_0^t -k_{ci}\Delta i_{d_offset}dtd\theta_e = \frac{k_{ci}}{\omega_e}\left(\Delta i_a - \Delta i_b\right) \\
\sec IV &= \int_{\frac{2\pi}{3}}^{\pi}\int_0^t -k_{ci}\Delta i_{d_offset}dtd\theta_e = -\frac{k_{ci}}{\omega_e}\Delta i_b \\
\sec VI &= \int_{\frac{5\pi}{3}}^{2\pi}\int_0^t -k_{ci}\Delta i_{d_offset}dtd\theta_e = \frac{k_{ci}}{\omega_e}(\Delta i_a + \Delta i_b)
\end{aligned} \tag{12}$$

From equation (12):

$$\begin{aligned}
\varepsilon_a &= \sec IV - \sec I \\
\varepsilon_b &= \sec III - \sec VI \\
\varepsilon_2 &= \varepsilon_a + \varepsilon_b = -4\frac{k_{ci}}{\omega_e}\Delta i_b
\end{aligned} \tag{13}$$

Similarly, controlling Eq. (13) to zero eliminates the effect of the B phase offset error on the phase current measurement results.

When the offset error is zero, then the result of integrating Eq. (8) for each $\pi/3$ electrical angle satisfies Eq. (14).

$$\begin{aligned}
\sec I &= \sec IV \\
\sec II &= \sec V \\
\sec III &= \sec IV
\end{aligned} \tag{14}$$

III. C. 3) Gain Error Calculation

When K_a and K_b are equal, Eq. (14) is zero, i.e., there is no gain error in the dq axis. Therefore, when K_a and K_b are not equal, Eq. (15) reflects the gain error.

$$\begin{aligned}
\sec I = \sec IV &= \int_0^{\frac{\pi}{3}}\int_0^t -k_{ci}\Delta i_{d_scale}dtd\theta_e = 0 \\
\sec II &= \int_{\frac{\pi}{3}}^{\frac{2\pi}{3}}\int_0^t -k_{ci}\Delta i_{d_offset}dtd\theta_e = -\frac{3k_{ci}(K_b - K_a)I}{8\sqrt{3}\omega_e} \\
\sec III &= \int_{\frac{2\pi}{3}}^{\pi}\int_0^t -k_{ci}\Delta i_{d_scale}dtd\theta_e = \frac{3k_{ci}(K_b - K_a)I}{8\sqrt{3}\omega_e}
\end{aligned} \tag{15}$$

From equation (15):

$$\begin{aligned}
\varepsilon_x &= \sec I - \sec II \\
\varepsilon_y &= \sec III - \sec IV \\
\varepsilon_3 &= \varepsilon_x + \varepsilon_y = \frac{3k_{ci}(K_b - K_a)I}{8\sqrt{3}\omega_e}
\end{aligned} \tag{16}$$

III. C. 4) Phase current compensation

Since $i_d^* = 0$, the closed-loop regulation of current makes $i_d = -i_d^m$, which also contains offset error and gain error, so the error amount can be found out by integrating i_d, and the measurement error can be eliminated by adding the closed-loop regulation of the error amount in the original vector control system. The error compensation algorithm is shown in Fig. 2.

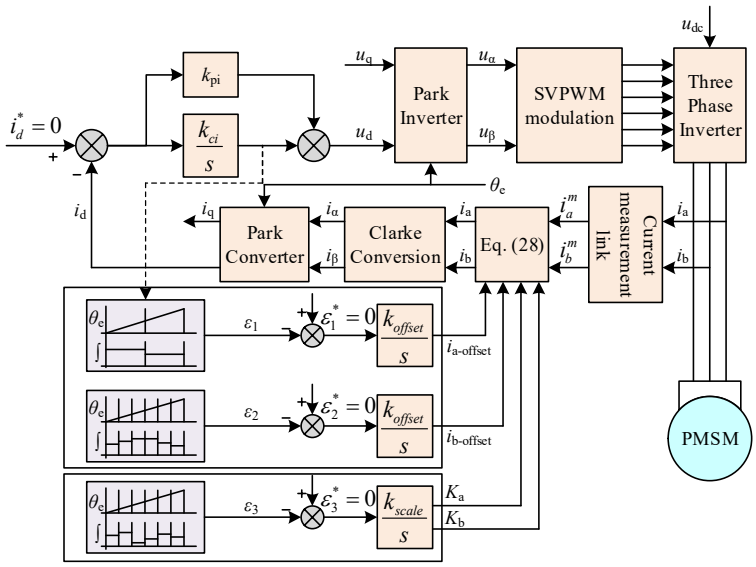

Figure 2: Error compensation algorithm

IV. Simulation and experimental verification

IV. A. Error Compensation and Interference Suppression Verification

IV. A. 1) Verification of error compensation effect

In order to verify the compensation effect of this paper's monitoring system on the current measurement error compensator, Matlab/Simulink software is used to simulate the SPMSM system. The parameters in the simulation model are set as follows: the rated power of the permanent magnet synchronous motor is 450 W, the rated current is 25 A, the rated rotational speed is 2200 r/min, the stator resistance is 0.073 Ω, the stator inductance is 0.00037 H, the flux of the permanent magnets is 0.01406 Wb, the number of pole pairs is 12, the dc-side voltage of the three-phase voltage-type inverter is 48 V, the current PI regulator's cutoff frequency is ωc =2513 rad/s, the frequency of SVPWM modulation module is 20 kHz, the cutoff frequency of low-pass filter LPF is 314 rad/s, the coefficient of integrator is k_i =10, and the command values of the d and q axis stator currents are i_d^* =0 and i_q^* =5A, and the error signal of 0.25 A is injected into phase a and phase c. The current measurement error compensator is put into operation at 2s, and the simulated waveform is shown in Fig. 3, with Δi_{dm}, Δi_{qm} /A denoted as S1; $\Delta i_{\alpha m}$, $\Delta i_{\beta m}$ /A is denoted as S2; $\Delta i_{\alpha m}$, $\Delta i_{\beta m}$ /A is denoted as S3.

The waveforms in the figure are, from top to bottom: $d-q$ stator current measurement error in synchronous rotating coordinate system Δi_{dm}, Δi_{qm}, $\alpha-\beta$ stator current measurement error in stationary coordinate system $\Delta i_{\alpha m}$, $\Delta i_{\beta m}$, $\alpha-\beta$ Estimated value of stator winding phase current measurement error in stationary coordinate system $\Delta i_{\alpha m}$, $\Delta i_{\beta m}$, and motor torque T. As can be seen from the simulated waveforms: the stator current measurement error in the $d-q$ synchronous rotating coordinate system is an AC signal, and the stator current measurement error in the $\alpha-\beta$ stationary coordinate system after Park inversion is a DC signal; During (0 to 2) s, the current measurement error compensator does not operate, the estimated value of the current measurement error is 0, and there is a significant pulsation in the motor torque. After the current measurement error compensator is put into operation at 2s, both the $d-q$ axis current measurement error and the α-β axis current measurement error gradually decrease and tend to zero, and the estimated value of the current measurement error gradually increases and tends to stabilize, and the stabilized values are $\Delta i_{\alpha m}$ =0.26A, $\Delta i_{\beta m}$ =-0.44A, and the pulsation of the motor torque is obviously reduced, and the stabilized value of the torque is T=0.67Nm, the simulation results are fully consistent with the theoretical analysis.

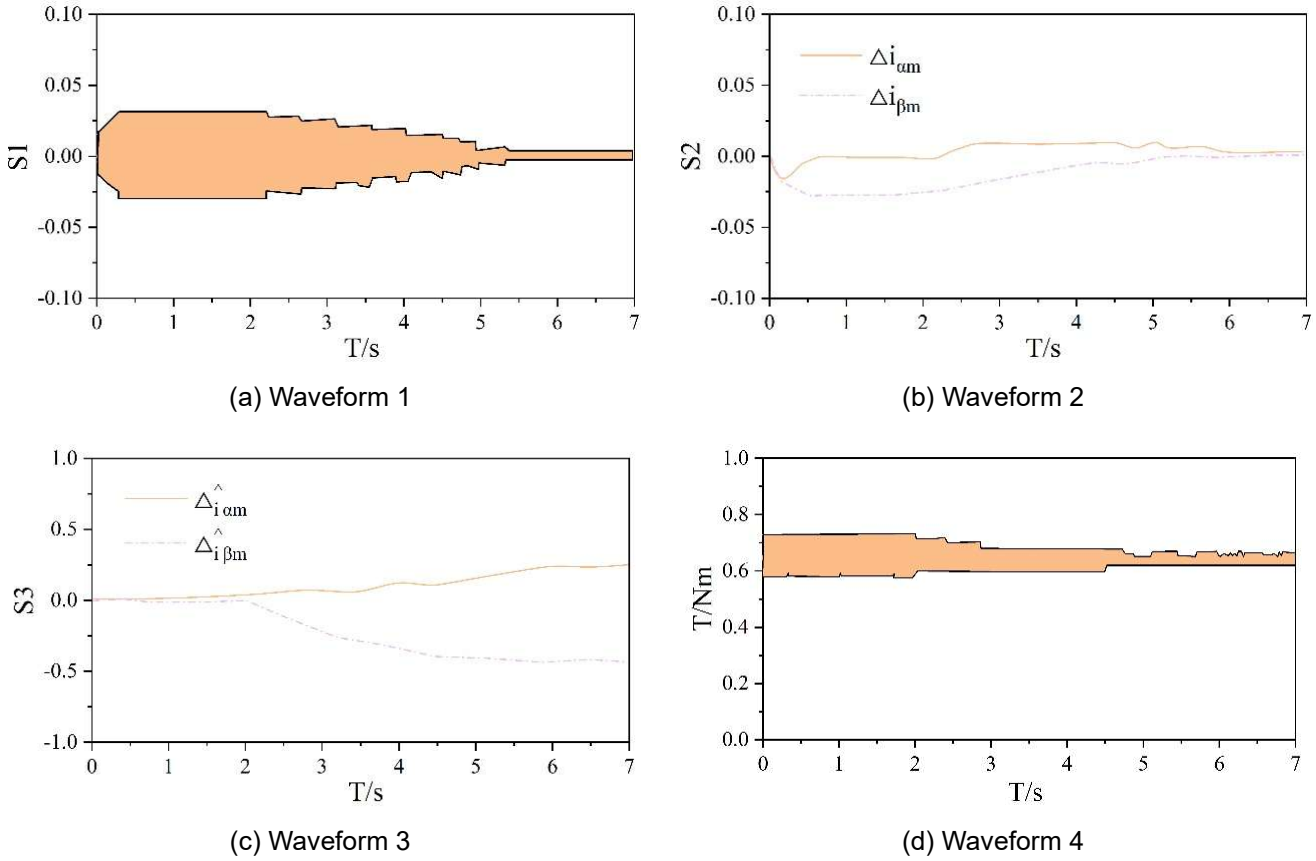

Figure 3: System simulation waveform

IV. A. 2) Verification of outer loop interference suppression

In order to verify the anti-interference ability of the current measurement error compensator to the outer-loop controller, the measurement error compensator in the simulation model corresponding to Fig. 4 is put into operation at 0s, and the command value of the q-axis stator current i_q^* is increased from 5A to 7A at 2s, and the rest of the parameters are kept unchanged, so that the simulation waveforms shown in Fig. 4 are obtained.

From the simulation waveform, we can see that after increasing the command value of q-axis stator current i_q^* from 5A to 7A at 2s, the measurement errors of $d-q$ axis current $\Delta i_{\alpha m}$, $\Delta i_{\beta m}$ and $\alpha-\beta$ axis current measurement errors $\Delta i_{\alpha m}$, $\Delta i_{\beta m}$ are almost unaffected after transient perturbations, and all of them are gradually decreasing and converging to zero; the estimated values of the current measurement errors are gradually increasing and converging to stable values, and the stable values are respectively, are $\Delta i_{\alpha m}$=0.27A, $\Delta i_{\beta m}$=-0.45A, exactly the same as when the current command i_q^*=5A in Fig. 4. At 2s, as the current command value i_q^* increases from 5A to 7A, the motor torque increases suddenly, and after that, the torque pulsation continues to decrease, and is finally stabilized at T=0.93Nm. The simulation waveforms show that the current error compensator can effectively inhibit the outer loop controller's interference, and the SPMSM system based on current measurement error compensator has good dynamic control performance.

IV. B. Simulation verification of compensation effect

In order to verify the dynamic and static performance of the current error compensation method, this section builds a model of vector control system of permanent magnet synchronous motor based on MATLAB/Simulink, and the motor parameters are shown in Table 1.

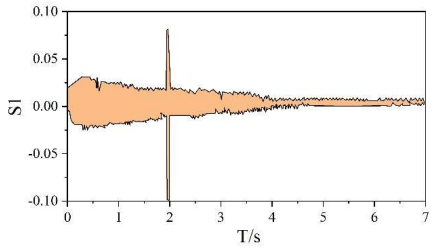

(a) Waveform 1

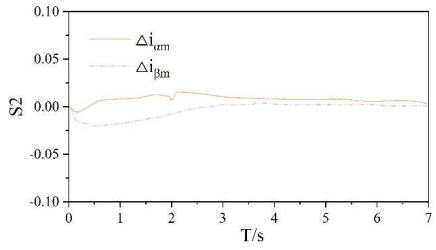

(b) Waveform 2

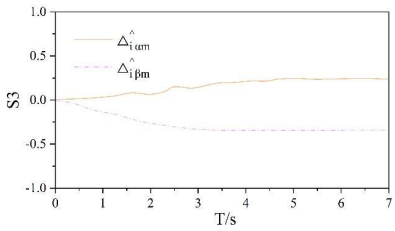

(c) Waveform 3

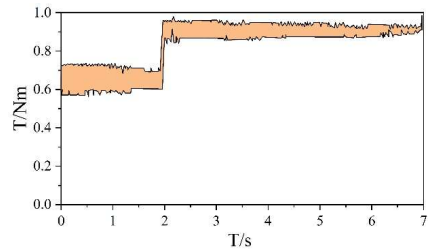

(d) Waveform 4

Figure 4: Anti-external ring interference simulation waveform

Table 1: Simulation motor parameter

Parameter	Numerical value	Parameter	Numerical value
Rated voltage U_e / V	210	Rated torque $T_e / (N \bullet M)$	6
Rated power P_e / W	755	Rated speed $n_e / (r \bullet \min^{-1})$	755
Stator resistance R_s / Ω	1.8	Stator inductance L_s / mH	0.842
Polar logarithm p	5		

The simulation model adopts the vector control strategy of permanent magnet synchronous motor with id=0. Firstly, it is verified that the gain error and offset error in the theoretical analysis will cause the speed and torque of the motor to pulsate in f_e and $2f_e$, and the simulation conditions are set up as follows: k_a=1.1, k_a=0.9, Δi_{a_offset} =0.03, Δi_{b_mea} =0.05. Then the stator current compensation algorithm is added to the simulation model, and it is verified that the compensation algorithm eliminates the speed and torque pulsations caused by the current measurement error.

Fig. 5 shows the rotational speed graph of the motor running stably at the speed of 325 r/min, and the motor speed has a periodic pulsation at 325 r/min, and the FFT analysis of the rotational speed is done, as shown in Fig. 6. The rotational speed contains f_e and $2f_e$ pulsation frequencies.

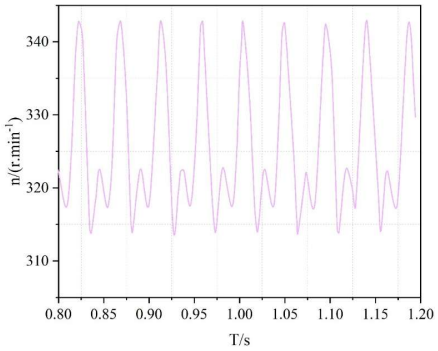

Figure 5: Transient motor speed

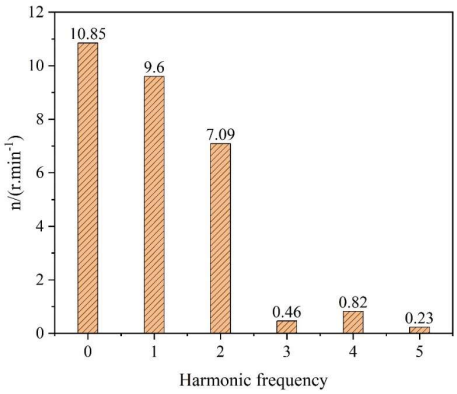

Figure 6: Steady state speed FFT analysis

Fig. 7 shows the comparison of rotational speed with and without current error compensation algorithm. It can be seen from the figure that the pulsation in the rotational speed is eliminated after the error current compensation. Further FFT analysis of the rotational speed obtained after compensating the current is done as shown in Fig. 8, which shows that the content of 1x angular frequency and 2x angular frequency is cut down drastically.

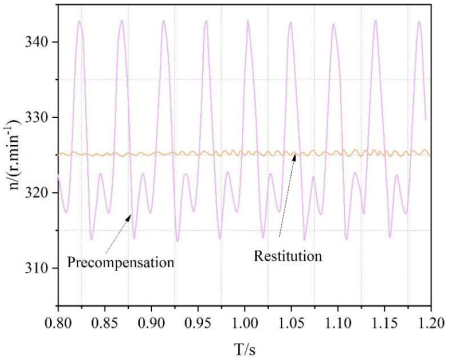

Figure 7: Before compensation, compensation is compared with the steady state speed

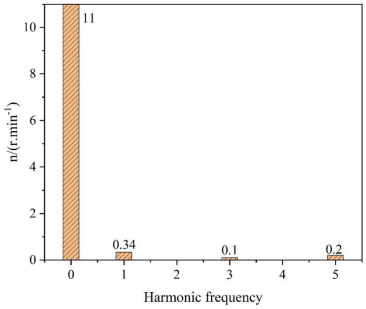

Figure 8: The compensation is analyzed after the steady speed FFT

In order to verify the dynamic performance of the algorithm, the load is increased by 2 N-m, while the given speed of the motor is increased at 3 s. The speed profile is shown in Fig. 9. The motor speed increases from 325r/min to 55r/min in 3s, and there is obvious speed jitter in the speed curve without the error current compensation method, while the speed pulsation phenomenon is basically eliminated in the simulation experiment with the current compensation method, which proves that the algorithm has better dynamic performance.

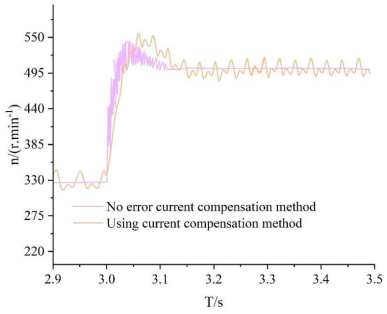

Figure 9: Dynamic speed graph

V. Conclusion

The study proposes an error control monitoring system based on current measurement, and in order to minimize the influence of the measurement error on motor control, a compensation strategy for segmental integration of the d-axis current is proposed. It is analyzed by simulation and experiment, and the experimental results show that the monitoring system eliminates the interference of the outer-loop controller, improves the dynamic control capability of the current measurement error compensator, and the compensation strategy can better suppress the speed pulsation caused by the current measurement error, which proves the effectiveness and good dynamic performance of the monitoring system and compensation strategy proposed in this paper.

Acknowledgements

This work was supported by State Grid Corporation Technology Project (5700-202219210A-1-1-ZN).

References

[1] Cetina, R. Q., Roscoe, A. J., & Wright, P. S. (2017, August). A review of electrical metering accuracy standards in the context of dynamic power quality conditions of the grid. In 2017 52nd International Universities Power Engineering Conference (UPEC) (pp. 1-5). IEEE.

[2] Apse-Apsitis, P., Vitols, K., Grinfogels, E., Senfelds, A., & Avotins, A. (2018). Electricity meter sensitivity and precision measurements and research on influencing factors for the meter measurements. IEEE Electromagnetic Compatibility Magazine, 7(2), 48-52.

[3] O'driscoll, E., & O'donnell, G. E. (2013). Industrial power and energy metering–a state-of-the-art review. Journal of cleaner production, 41, 53-64.

[4] Cetina, Q., Roscoe, R. A. J., & Wright, P. S. (2017, September). Challenges for smart electricity meters due to dynamic power quality conditions of the grid: A review. In 2017 IEEE International Workshop on Applied Measurements for Power Systems (AMPS) (pp. 1-6). IEEE.

[5] van den Brom, H. E., van Leeuwen, R., Marais, Z., ten Have, B., Hartman, T., Azpúrua, M. A., ... & Leferink, F. (2021). EMC testing of electricity meters using real-world and artificial current waveforms. IEEE transactions on electromagnetic compatibility, 63(6), 1865-1874.

[6] Leferink, F., Keyer, C., & Melentjev, A. (2016). Static energy meter errors caused by conducted electromagnetic interference. IEEE electromagnetic compatibility magazine, 5(4), 49-55.

[7] Diahovchenko, I., Dolník, B., Kanálik, M., & Kurimský, J. (2022). Contemporary electric energy meters testing under simulated nonsinusoidal field conditions. Electrical engineering, 1-16.

[8] Moret, F., & Pinson, P. (2018). Energy collectives: A community and fairness based approach to future electricity markets. IEEE Transactions on Power Systems, 34(5), 3994-4004.

[9] Morello, R., De Capua, C., Fulco, G., & Mukhopadhyay, S. C. (2017). A smart power meter to monitor energy flow in smart grids: The role of advanced sensing and IoT in the electric grid of the future. IEEE Sensors Journal, 17(23), 7828-7837.

[10] Frigo, G., & Braun, J. (2022, May). Measurement setup for a dc power reference for electricity meter calibration. In 2022 20th International Conference on Harmonics & Quality of Power (ICHQP) (pp. 1-5). IEEE.

[11] Bartolomei, L., Cavaliere, D., Mingotti, A., Peretto, L., & Tinarelli, R. (2020). Testing of electrical energy meters subject to realistic distorted voltages and currents. Energies, 13(8), 2023.

[12] Węgierek, P., & Konarski, M. (2016). The temperature effect on measurement accuracy of the smart electricity meter. Przegląd Elektrotechniczny, 92(8), 148-150.

[13] Wang, Y., Yu, W., Zhang, C., Ye, L., Wei, W., & Yang, Z. (2025). Design of On-Site Calibration Device for Electricity Meter Based on Pulse Detection. Inventions, 10(1), 6.

[14] Urekar, M., Pejic, D., Vujicic, V., & Avramov-Zamurovic, S. (2017). Accuracy improvement of the stochastic digital electrical energy meter. Measurement, 98, 139-150.

[15] Abate, F., Carratù, M., Liguori, C., & Paciello, V. (2019). A low cost smart power meter for IoT. Measurement, 136, 59-66.

[16] Fares Al Mohamad,Leonhard Donle,Felix Dorfner,Laura Romanescu,Kristin Drechsler,Mike P Wattjes... & Keno Kyrill Bressem. (2025). Open-source Large Language Models can Generate Labels from Radiology Reports for Training Convolutional Neural Networks. . Academic radiology,32(5),2402-2410.

[17] Hongbiao Xiang,Yanming Cao,Xu Cheng,Xianghong Zhao,Jiahao Lu,Yuexin Zhang... & Mian Zhang. (2025). Error compensation and precise tracking control of magnetic miniature swimmers via inverse modeling with deep neural networks. Journal of Magnetism and Magnetic Materials,621,172936-172936.